IEEE Access
Multidisciplinary | Rapid Review | Open Access Journal

Received 24 January 2023, accepted 28 February 2023, date of publication 6 March 2023, date of current version 9 March 2023.

Digital Object Identifier 10.1109/ACCESS.2023.3252581

RESEARCH ARTICLE

Analysis of the Topology and Electromagnetic Characteristics of Novel Stator Partitioned Axial Flux Disk Generator for Vehicles

LINTAO LI, LIWEI SHI, ZHENGWEI LIU, WENQIANG WANG, AND FACHENG LI
National Local Joint Engineering Research Center of Intelligent Power Integration Technology for Electric Vehicles, Shandong University of Technology, Zibo 255049, China

Corresponding author: Liwei Shi (liwei10@nuaa.edu.cn)

This work was supported in part by the National Natural Science Foundation of China under Grant 51975340 and Grant 51875327.

ABSTRACT Internal combustion engines emit high-temperature, high-pressure, and high-speed exhaust gases, resulting in wasted energy and low thermal efficiency. In order to recover the available residual energy in the exhaust gas, this paper proposes a new topology of the disk-type axial flux stator-excited doubly salient generator (AFSDSG) with partitioned stator suitable for high-temperature and high-speed operation. Based on the analysis of the above generator inductance characteristics, the influence mechanism of three pole-slot structures on the induced electromotive force (IEMF) of the armature winding is clarified, the equivalent magnetic circuit method is used to analyze the influence of different winding arrangements on the no-load performance of the generator, and the principles of pole-slot structure optimization and winding arrangement are summarized. The finite element software is used to model and simulate different configuration. After focusing on the analysis of transient characteristics such as inductance, armature winding IEMF, and air-gap flux, it is concluded that different from the conventional pole-slot structure and winding connection method make that only the overlapping area of the stator and the rotor changes linearly can produce a constant voltage, the winding arrangement of Winding Partition Excitation Span 2 has a high IEMF amplitude value and low harmonic content. Finally, the prototype of a three-phase 12/8-pole was trial manufactured and tested. The consistency of the simulation results and experimental results is verified the innovation and feasibility of the new topology proposed in this paper.

INDEX TERMS Disk-type generator, axial flux, pole-slot structure, windings connection.

I. INTRODUCTION

Improving performance and saving energy are the eternal development themes of the automobile and motor industries. The energy generated by the combustion of fuel in internal combustion engines is mainly converted into mechanical energy for output, cooling energy, exhaust energy, and mechanical loss energy. The traditional internal combustion engine is inefficient, and a large amount of fuel energy is lost or directly discharged into the atmosphere, which not only wastes resources, but also causes damage to the environment [1], [2].

In order to improve the thermal efficiency of internal combustion engines, many scholars have conducted extensive research [3], [4], [5], [6]. Recovering exhaust gas energy and reducing the share of exhaust gas loss energy is one of the research hotspots for improving thermal efficiency [7]. Turbine power generation uses the energy of the exhaust gas to drive the rotation of the exhaust gas turbine, thus allowing the rotor of the generator coaxial to it to rotate and generate electrical energy for energy conversion.

However, more research has been carried out on the rationality of turbine power generation systems [8], [9], [10], and less on the structure of the generator body. In reality, nevertheless, the harsh operating environment of the turbocharger places high demands on the generator.

The associate editor coordinating the review of this manuscript and approving it for publication was Abderrezak Rachedi.

The magnetic field in a generator can be provided by both permanent magnets and excitation windings. The advantages of high performance of permanent magnets have made permanent magnet synchronous motors one of the hot research topics in motors [11], [12]. Scholars have extensively and intensively studied the structure of motor ontology [13], [14]. For example, Korean scholar has proposed a new spoke-type permanent magnet synchronous generator, which reduces the leakage flux and the cogging torque through a special design of the isolation bridge and support structure [15]. However, the high temperature characteristics of turbochargers increase the risk of demagnetization of the permanent magnets exponentially, making the supply of the magnetic field through the excitation winding the best option.

In conventional radial flux wound excitation generators, the conference [16] proposes a generator in which the armature current and the stator harmonic control winding current jointly generate the excitation power, the former compensating for the weak magnetic effect produced by the armature reaction to keep the load voltage stable. The conference [17] proposes a permanent magnet synchronous generator with three sets of excitation windings, one set on the stator and two sets on the rotor. The excitation winding on the stator generates a magnetic field that produces an AC voltage in the first rotor excitation winding, which is rectified by a diode to provide a DC excitation current to the second rotor excitation winding. The generator has proven to have a hard external characteristic and a THD of less than 5% for both no-load and load output voltages.

Radial flux wound excitation generators are favored for their ease of regulation and control [18], [19], but the axial length is an important influence on the output power, the greater the axial length, the greater the output power. But in fact, a larger axial length will contribute to a larger rotating mass, which has an adverse impact on the response of the turbocharger. Axial flux generators with stable construction and small mass rotors are therefore the preferred choice for high speed operation.

The double-sided stator middle rotor is one of the basic structural forms of axial flux generators, with a small axial rotor length and small rotating mass, in line with the original design objectives. The existing literature has only studied axial flux PMGs in some detail [20]. The conference [21] studied the Halbach axial flux permanent magnet generator, comparing the effect of different parameters such as pole arc coefficient and air gap length on the total harmonic distortion. In [22], the pole shape was analyzed and the results showed that the triangular pole has a higher back electromotive force (EMF) and output power. The conference [23] proposed a radial-axial flux switched permanent magnet generator with both stators. One stator is similar to the conventional radial flux internal stator and the other is similar to the axial flux motor stator consisting of U-shaped stator modules, both of which are spatially perpendicular and the flux is closed after passing through the rotor. It has the advantage of being noiseless, flux concentrated and a passive rotor. The overly prominent advantages of permanent magnets have allowed the inherent property of the excitation winding easy to adjust magnetic field and suitability for high temperatures to be overlooked, so little research has yet been reported on winding-excited disk generators. Based on the above analysis, a summary of the existing research is shown in Table 1.

TABLE 1. Summary of existing research.

Excitation method	Direction of magnetic flux	Advantages	Disadvantages
Permanent magnets	Radial[24], [25]	High efficiency, high power density	Easy demagnetization at high temperatures
	Axial[26]	Compact structure, high torque density	
	Radial-axial[23]	High space utilization and high power density	Complex magnetic circuit and difficult prototype manufacture
Winding excitation	Radial[27]	Convenient and easy to control voltage regulation	Large rotor axial length and high rotational inertia
	Axial	Small axial length and low rotor mass	High magnetic resistance

As for the segmented rotor, it is widely used in radial flux switched reluctance motors [28] and to a lesser extent in some axial flux motors [29], but its sectorial rotor is permanent magnets. For example, reference [30] proposed a dual-stator single-rotor axial flux hybrid excitation generator with armature winding in the stator yoke and excitation winding in the stator teeth, a rotor sandwiched between two stators, and a rotor frame with fan-shaped magnetic poles affixed on both sides, and the rotor slots formed by their adjacent poles are parallel slots. Besides, it has also been reported in the dual-rotor single-stator machine [31]. In contrast, for the axial flux dual-stator single-rotor machine, the non-permanent magnet sectorial segmented rotor is the first application, and the rotor slots are also sectorial, which is different from the parallel slots in the conference [30]. When it comes to partitioned stators, it is not the traditional concept of an E-type or C-type stator, as described in references [31], [32], but rather a distinction of functional areas that define the name of the stator according to the role of the windings wound on the stator. In fact, dual-stator single-rotor motors inherently have two stators, but none of the previously reported research work has seen the representation of stator partitions, which means that non-partitioned-stator increases the cost and installation complexity of the machine. For example, reference [33] reported an axial flux dual-stator single-rotor permanent magnet starter generator with the rotor sandwiched between the two stators as in reference [30]. To improve its thermal performance, the permanent magnets are segmented radially

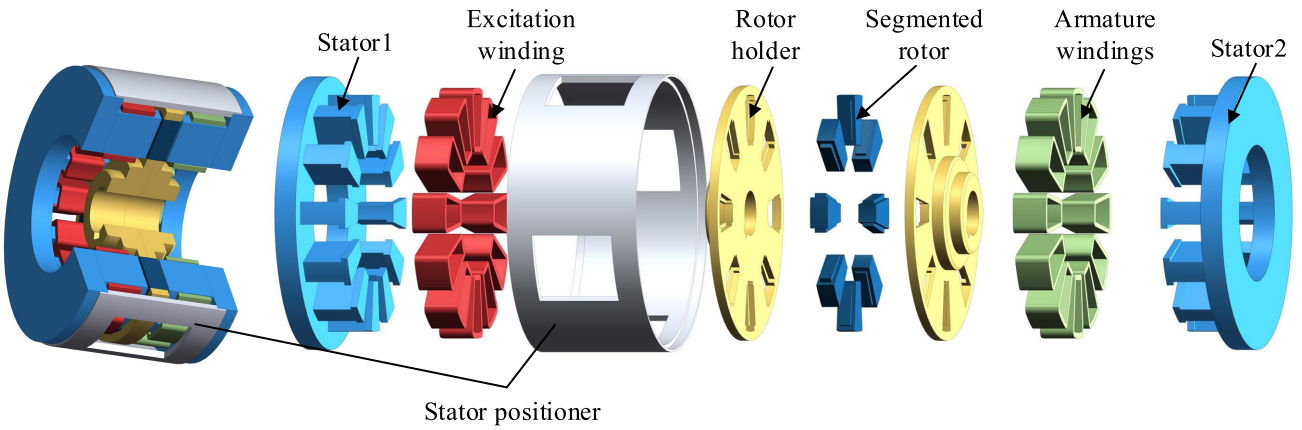

FIGURE 1. The structure of the designed AFSDSG.

to suppress their losses and the separated rotor cover also dissipates heat efficiently.

In response to the above analysis, this paper proposes a stator axially partitioned axial flux stator-excited doubly salient generator (AFSDSG) topology. The generator has a robust rotor with a small mass, which reduces the rotational inertia and is not affected by the working environment of the turbocharger. This paper describes the generation mechanism of induced electromotive force (IEMF) and the ideal changing waveform of armature winding inductance and IEMF. According to the different relative positions of the stator and rotor, the mathematical model of the overlapping area of the stator and rotor of three pole-slot structures is established by synthesizing the principle that the magnetic flux density of the air gap changes with the presence. The linear variation of the overlapping area of the sectorial pole sectorial slot (SPSS) makes the flux linkage vary uniformly, which greatly reduces the output voltage ripple. Combined with the analysis of the winding arrangement, the result of IEMF with less harmonics and high amplitude is obtained. Besides, the static and dynamic characteristics of the AFSDSG are also obtained by means of finite element software. Finally, a prototype is manufactured, and the IEMF of the prototype is tested. Compared with the simulation results, the feasibility and innovation of the proposed AFSDSG are verified.

II. AFSDSG STRUCTURE AND PRINCIPLE

The designed AFSDSG is shown in Fig. 1. The segmented rotor is fixed in the non-magnetic rotor frame and sandwiched between two symmetrical stators. The field winding and armature winding are wound on the stator teeth in a certain order. A direct current (DC) is fed into the excitation winding to establish the internal magnetic field of the machine. The rotor rotates under the drive of the prime mover to generate the IEMF by the flux linkage which regularly appears in the armature winding.

When the armature winding and the field winding are partitioned synchronously with the stators, the field winding is wound across both poles and the armature winding is

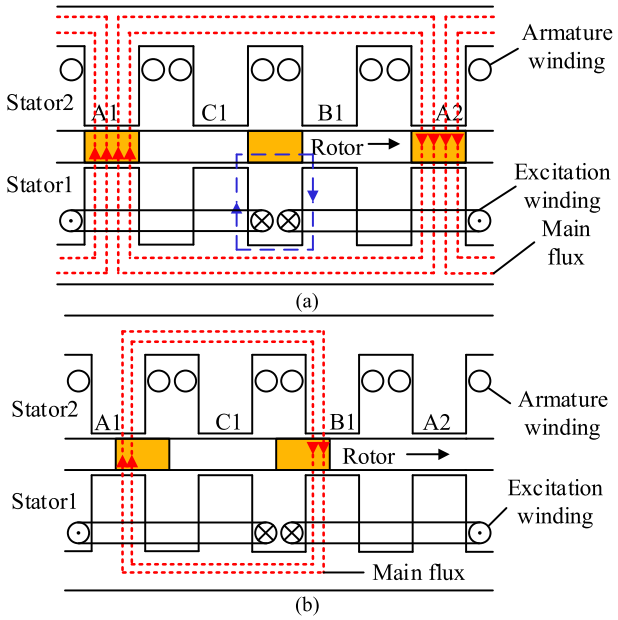

FIGURE 2. Flux paths at different rotor positions, (a) 0° mechanical angle (0° electrical angle); (b) 7.5° mechanical angle (7.5° electrical angle).

wound centrally, as shown in Fig. 2. This figure is a schematic diagram of the axial cross-sectional flux at the radial middle radius of the AFSDSG. The rotor flushing phase A is defined as 0° mechanical angle. When the rotor teeth are located at this position, the flux linkage appears in the phase A after passing through the rotor teeth and the air gap. At the same time, it is the maximum flux of the phase, as shown in Fig. 2 (a). The rotor rotates anticlockwise by 7.5° mechanical angle, as shown in Fig. 2 (b). Compared to the 0° position, the flux in phase A decreases and the flux in phase B increases, i.e. the inductance of phases A and B change simultaneously. When the DSG2 power generation method is used, within the process of 0° to 7.5°, phase A and B work at the same time to generate power, the ideal inductance and IEMF waveform are shown in Fig. 3. The main flux linkage is closed after passing

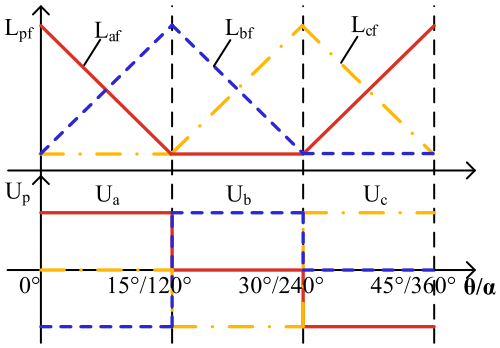

FIGURE 3. Ideal inductance and IEMF.

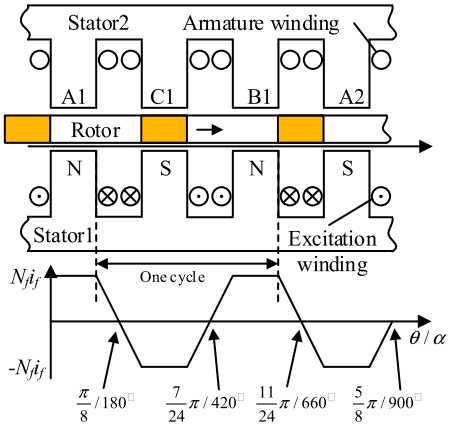

FIGURE 4. Distribution of excitation potential.

through the stator and rotor iron cores with air gaps, showing a circulation in the axial and circumferential directions. θ and α indicate the mechanical and electrical angles respectively in Fig. 3 and Fig. 4.

A magnetic field is established in the stator 1 after the DC is applied to the excitation winding. The rotor continues to rotate under the drive of the prime mover, and the magnetic flux is regularly induced in the armature winding to generate IEMF. However, in reality, as the rotor rotates, the magnetic flux in the excitation winding changes from moment to moment, which consequently contributes to periodically changes in the excitation self-inductance. The excitation back EMF and excitation positioning torque caused by excitation self-inductance are represented by U_f and T_f, respectively. Therefore, the expressions of the two are as follows:

$$\begin{cases} T_f = \dfrac{1}{2} i_f^2 \dfrac{dL_f}{d\theta} \\ U_f = -\dfrac{d\psi_f}{dt} = -L_f \dfrac{di_f}{dt} - i_f \dfrac{di_f}{dt} \end{cases} \tag{1}$$

where i_f is the excitation current and L_f is the field winding self-inductance.

It can be seen from the above formula that the excitation back EMF U_f and the excitation positioning torque T_f are related to the excitation current i_f and the excitation self-inductance L_f. When the excitation current remains unchanged, the two are only related to the excitation self-inductance L_f. Nevertheless, the excitation self-inductance is caused by the periodic change of the flux linkage in the excitation winding during the rotor rotation. Accordingly, the following factors should be considered in the arrangement of the stator and rotor teeth and windings on the performance of the machine:

(1) During the working process of the generator, the excitation self-inductance should not change significantly with the rotor rotation, and the excitation back EMF and positioning torque should tend to be close to 0.

(2) The total magnetic permeability of the generator should remain constant at any moment, the magnetic voltage drop in each magnetic circuit should be the same and the inductance of each phase should be symmetrical.

III. AFSDSG TOPOLOGY ANALYSIS

A. STRUCTURAL ANALYSIS OF THE POLES AND SLOTS

For the purpose of this analysis, the following assumptions are made.

(1) Ignore the effects of magnetic circuit saturation and eddy current effects.

(2) Ignore the effect of end effects on the winding.

(3) Ignore the effect of the third air gap.

The rotor rotates and the EMF induced by the armature winding of phase A is

$$e_a = -\frac{d\varphi_a}{dt} - N\frac{d\phi_a}{dt} \tag{2}$$

$$\phi_a = B_z(\theta) S_a(\theta) \tag{3}$$

where φ_a is the flux linkage of phase A, N is the number of turns of the phase winding, ϕ_a is the flux in each turn of the coil, $B_z(\theta)$ is the axial air gap flux of the excitation stator pole, and $S_a(\theta)$ is the stator-rotor overlapping area. And the latter two are functions of the rotor position angle θ. Thus, the phase IEMF is positively correlated with the rate of change of the phase flux linkage.

$$B_z(\theta) = \mu H(\theta) \tag{4}$$

$$H(\theta) = F(\theta)/[h_g(\theta)] \tag{5}$$

$$B_z(\theta) = \mu_0 F(\theta) \Lambda_g(\theta) \tag{6}$$

where μ is the permeability, $H(\theta)$ is the magnetic field strength, $F(\theta)$ is the excitation magnetic potential, $H_g(\theta)$ is the air gap length, and $\Lambda_g(\theta)$ is the air gap permeability, so the flux linkage is only related to the excitation potential and the stator-rotor overlapping area.

Taking the excitation of each pole as an example, the distribution of the excitation potential generated by the excitation winding is illustrated, as shown in Fig. 4. Since each stator pole of the stator 1 has an excitation winding, and the adjacent excitation windings are wound in opposite directions, the excitation magnetic field at the air gap between the stator 1 and the rotor will present an alternately distributed trapezoid shape. The mechanical angle occupied by each stator pole is

$\pi/12$. When the stator pole arc coefficient is 0.5, the mechanical angle occupied by a pair of excitation magnetic poles is $\pi/3$, and its peak value is $N_f i_f$, then the excitation magnetic potential can be expressed by the following formula:

$$F(\theta) = \begin{cases} N_f i_f, & 0 + \frac{mk}{3} < \theta \le \frac{\pi}{12} + \frac{mk}{3} \\ -\frac{24 N_f i_f}{\pi}(\theta - \frac{\pi}{8}), & \frac{\pi}{12} + \frac{mk}{3} < \theta \le \frac{\pi}{6} + \frac{mk}{3} \\ -N_f i_f, & \frac{\pi}{6} + \frac{mk}{3} < \theta \le \frac{\pi}{4} + \frac{mk}{3} \\ \frac{24 N_f i_f}{\pi}(\theta - \frac{7\pi}{24}), & \frac{\pi}{4} + \frac{mk}{3} < \theta \le \frac{(k+1)\pi}{3} \end{cases} \tag{7}$$

It can be seen from the above formula that the air-gap flux is a constant value under one excitation pole. As a consequence, the change of the phase-A flux linkage depends on the overlapping area of the stator and the rotor. Considering that the analysis of the above inductance characteristics, design requirements and the determinants of the phase IEMF, three pole-slot structures can be shown in Fig. 5, namely, Parallel Pole Sectorial Slot (PPSS) and Sectorial Pole Parallel Slot (SPPS), and SPSS. α is the stator pole arc width, β is the stator pole pitch, and γ is the rotor pole arc width. The stator and rotor pole arc widths of the three pole-slot configurations are all the same, in accordance with the working mode shown in Fig. 3. The axial end faces of the stator and rotor poles have the same shape to ensure that the maximum amount of magnetic flux is conducted when the stator and rotor teeth are aligned.

The PPSS configuration is extended in light of the traditional radial flux SDSM. Its low slot space-factor contributes to a great waste of machine inner space. And, the small overlap area when the stator and rotor are aligned brings about the small inductance difference, which makes the IEMF generated by the armature absolutely small. The following solutions are available for the two problems of the PPSS configuration described above. It is called SPPS with fan-shaped teeth and parallel slots by increasing the mechanical angle of the outer diameter of the stator teeth of the PPSS and reducing the mechanical angle of the inner diameter of the stator teeth, which can accommodate more windings in the stator slots and solve the former problem of low slot space-factor of the PPSS configuration. For the latter, only increase the mechanical angle of the outer diameter of the stator teeth of the PPSS, which is called SPSS, so as to make the area larger. Since only the mechanical angle of the outer diameter of the stator teeth is changed, the slot space-factor of the SPSS is the same as that of the PPSS.

With low core loss as the constraint goal, it is necessary to prevent the formation of a closed magnetic flux loop between the rotor pole and the stator pole on the same side when the rotor is aligned with the stator slot. As a result, the PPSS uses the radial lines at both ends of the inner diameter of the teeth as the constraint boundary for the pole arc coefficient and the SPPS uses the radial lines at both ends of the outer diameter of the teeth to prevent losses due to the continuous flow of magnetic flux.

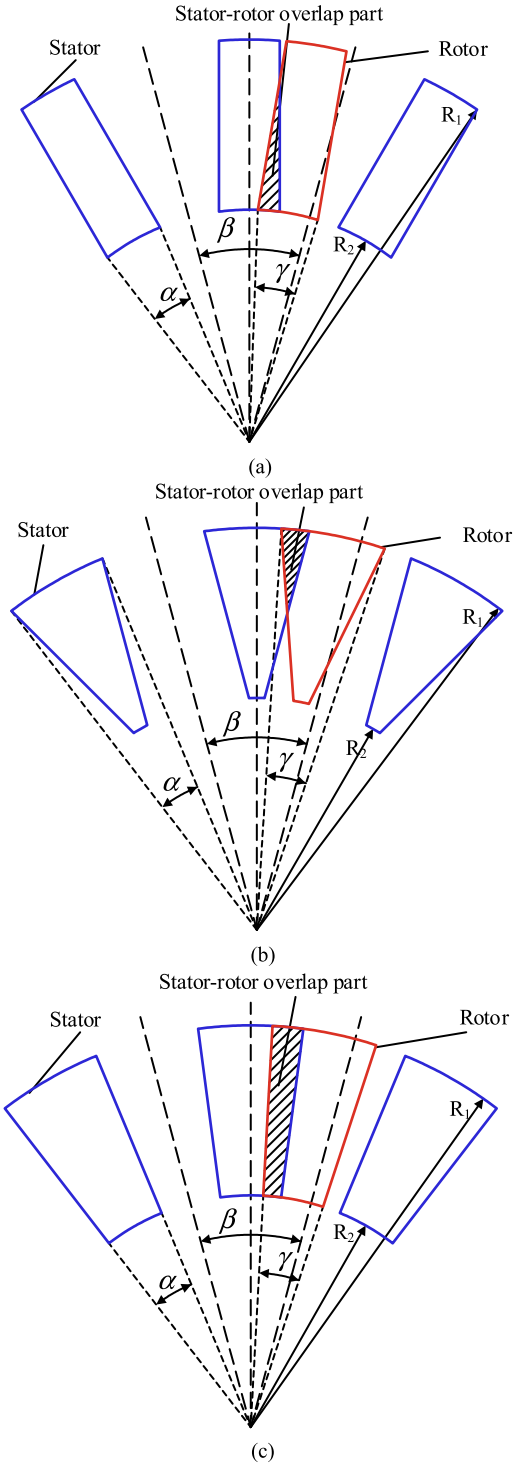

FIGURE 5. Three stator-rotor configurations, (a) PPSS; (b) SPPS; (c) SPSS.

In the rotor rotation process of PPSS and SPPS, the calculation methods of the stator-rotor overlap area are different before and after the typical position, as shown in Fig. 6,

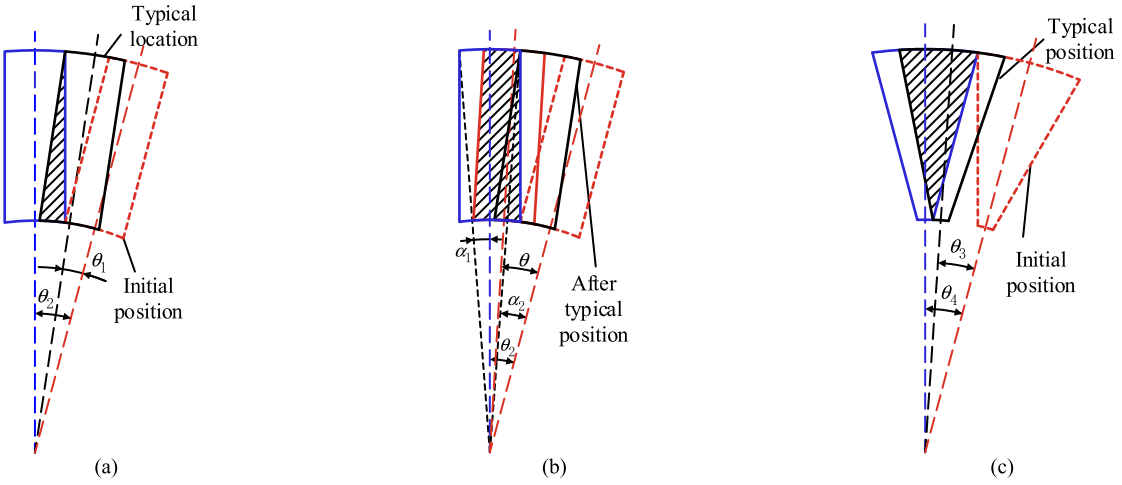

FIGURE 6. Typical positions for both configurations, (a) PPSS typical position; (b) After typical position of PPSS; (c) SPPS typical position.

so the overlap area should be calculated separately at these two positions.

The overlap area covered by PPSS can be expressed as: (8), shown at the bottom of the next page.

The overlap area covered by SPPS can be expressed as: (9), shown at the bottom of the next page.

The overlap area covered by PPSS can be expressed as:

$$S_{\mathrm{SPSS}} = \frac{\theta\pi\left(\mathrm{R}_1^2 - \mathrm{R}_2^2\right)}{360} \tag{10}$$

The r_1 in (8) and r_2 in (9) are the overlap radius of the overlap region before the typical positions of PPSS and SPPS respectively, and the curves are shown in Fig. 7 after the cubic polynomial fit.

Fig. 8 shows a graph of the overlap area of the three. The PPSS and SPPS show a curvilinear increase in their area before the typical position, mainly due to the fact that the overlap radius increases significantly with each unit angle of rotation of the rotor before the typical position, and the amount of increase in their overlap portion also increases gradually. After the typical position, the amount of increase in overlap area varies less per unit angle of rotor rotation and is overall linear in relation to the rotor angle. From (2) and (3), it can be seen that

$$\begin{aligned} \mathrm{e} &= -N\frac{\mathrm{d}\phi_{\mathrm{a}}}{\mathrm{d}t} = -NB_{\mathrm{z}}(\theta)\frac{\mathrm{d}S_{\mathrm{a}}(\theta)}{\mathrm{d}t} \\ &= -NB_{\mathrm{z}}(\theta)\frac{\mathrm{d}S_{\mathrm{a}}}{\mathrm{d}\theta}\frac{\mathrm{d}\theta}{\mathrm{d}t} \end{aligned} \tag{11}$$

From the above equation we can see that only when the overlapping area changes uniformly, will the generator generate a constant IEMF. The IEMF of the PPSS and the SPPS is on the rise before the typical position, whereas after the position, it is a certain value, which leads to the fact that the constant IEMF generated by the two accounts for a small electrical angle and has a large voltage pulsation.

Considering the above analysis, the arrangement of the stator pole-slot structure should follow two principles: one is that in the process of the rotor sliding in and out, the overlapping area of the stator and the rotor should be maintained unchanged to ensure that the armature winding generates a constant IEMF during the process. The other is that when the stator and rotor are aligned, the overlapping area should be as large as possible to increase the maximum phase inductance.

B. WINDING ARRANGEMENT

In an inductance cycle, the pole-slot structure affects the inductance change of the rotor slip-in and slip-out, which determines the change rate of the inductance. The winding arrangement affects the instantaneous state when the rotor aligns with the stator poles and slots, and also affects the direction of the internal magnetic circuit of the machine. These two moments are reflected on the flux linkage curve as the maximum value $\varphi_{\max}$ and the minimum value $\varphi_{\min}$ of the flux linkage.

When arranging the winding layout, the following principles should be met. On the basis that the magnetic chain rises, falls, and remains unchanged for 120° of electrical angle respectively, the flux conductance $\varphi_{\max}$ is increased as much as possible when the stator and rotor are flushed together, and the flux $\varphi_{\min}$ in the armature winding is reduced when the rotor is flushed together with the stator slot, i.e., the leakage is reduced to increase the armature winding induced electric potential amplitude.

The excitation winding and armature winding are wound on two stators, respectively. The excitation windings, concentrated windings, are wound in opposite directions to each other, called Winding Partitioning Excitation Span 1 (WPES1). Yet, when the rotor is aligned with the stator slots, the flux will pass through the rotor and form a closed loop between the two excitation stator poles of opposite polarity

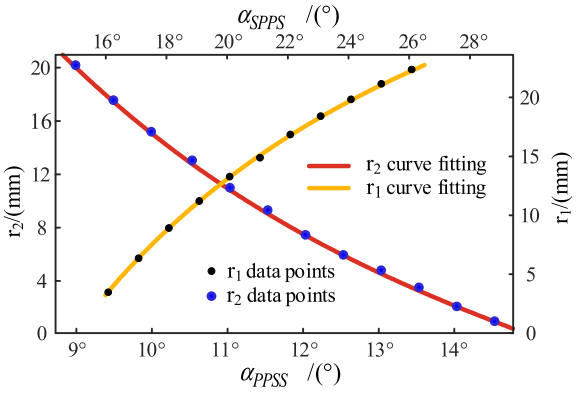

FIGURE 7. Overlap radius polynomial fit.

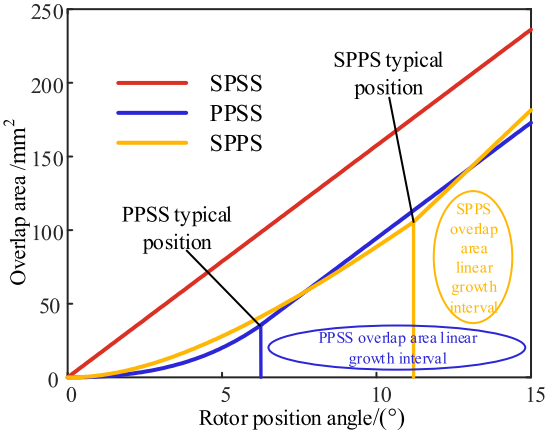

FIGURE 8. Overlap area variation curves.

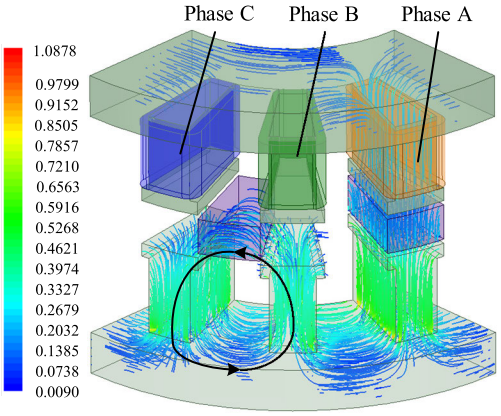

FIGURE 9. Leak flux distribution of WP-ES1.

due to the double salient, increasing the machine losses and reducing the motor performance, as shown in Fig. 9.

In order to solve the above-mentioned problem of magnetic flux leakage, this paper shows two solutions based on the SPSS, as shown in Fig. 10. Both the armature winding and excitation winding are concentrated windings, which are alternately distributed on each stator tooth, and the in-phase armature windings are symmetrically arranged on the two stators, which is called Excitation and Armature Alternation (EAA). It completely avoids the leakage flux in the field stator poles in the WP-ES1. When the armature winding and the excitation winding are respectively wound on two stators like the WP-ES1, the excitation winding is wound across two poles with the armature winding concentrated, which is called Winding Partitioning Excitation Span 2 (WP-ES2). Compared with WP-ES1, WP-ES2 has halved the number of adjacent stator teeth of opposite polarity, and halved the number of leakage flux between stator poles, which can effectively reduce the high core loss caused by the high-density closed flux.

Fig. 11 shows the equivalent magnetic circuit for the three winding arrangements. F, Φ_m, Φ_{li}, and Φ_{lo} are the equivalent magnetic potential source of the field winding, the main flux generated by the field winding, the internal leakage flux of the main magnetic flux, and the external leakage magnetic flux of the main magnetic flux, respectively. G_{msa}, G_{mse}, G_{mr}, and G_{mg} are all main flux equivalent magnetic conductivity of the armature tooth, field tooth, rotor pole, and air gap, respectively. G_{lsa}, Gl_{se}, G_{lr}, and G_{lg} are leakage flux equivalent magnetic conductivity, which are armature tooth conductivity, excitation tooth conductivity, rotor pole conductivity, and air gap conductivity respectively.

As can be seen from Fig. 11, WP-ES1 and WP-ES2 have similar main flux and leakage flux loops. One of the leakage fluxes of WP-ES2 has a large contribution to the armature winding magnetic chain, increasing the maximum value of

$$S_{\mathrm{PPSS}} = \begin{cases} \displaystyle\int_0^{15°-\theta} \frac{\pi r_1^2}{360} \mathrm{dw}, & 0 < \theta \le \theta_1 \\ \displaystyle\frac{1}{2}(\mathrm{R}_1 - \mathrm{R}_2)\left(\sqrt{2}\mathrm{R}_2\sqrt{1-\cos(\theta+\alpha_1-\alpha_2)} + \sqrt{2}\,R_1\sqrt{1-\cos\theta}\right), & \theta_1 < \theta \le \theta_2 \end{cases} \tag{8}$$

$$S_{\mathrm{SPPS}} = \begin{cases} \displaystyle\int_0^{15°+\theta} \frac{\pi r_2^2}{360} \mathrm{dw}, & 0 < \theta \le \theta_3 \\ \displaystyle\frac{(15°+\theta_3)\,\pi r(\theta_2)^2}{360} + \int_0^{\frac{(\theta-\theta_3)\pi R_2}{180}} (R_1 - R_2)\,\mathrm{dl}, & \theta_3 < \theta \le \theta_4 \end{cases} \tag{9}$$

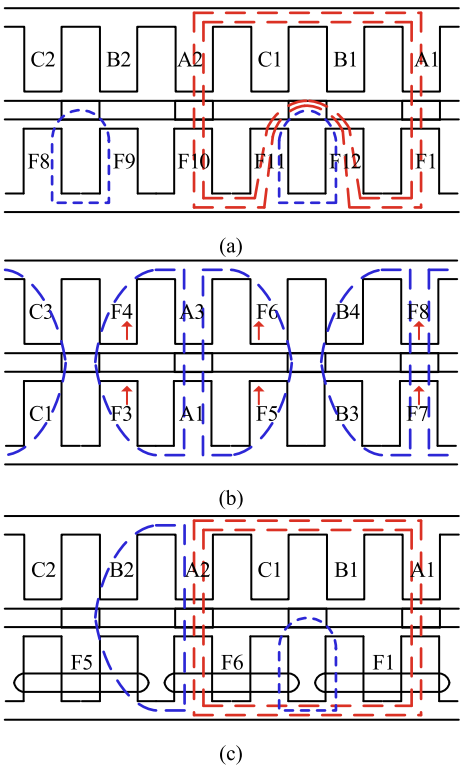

FIGURE 10. Three winding configurations, (a) WP-ES1; (b) EAA; (c) WP-ES2.

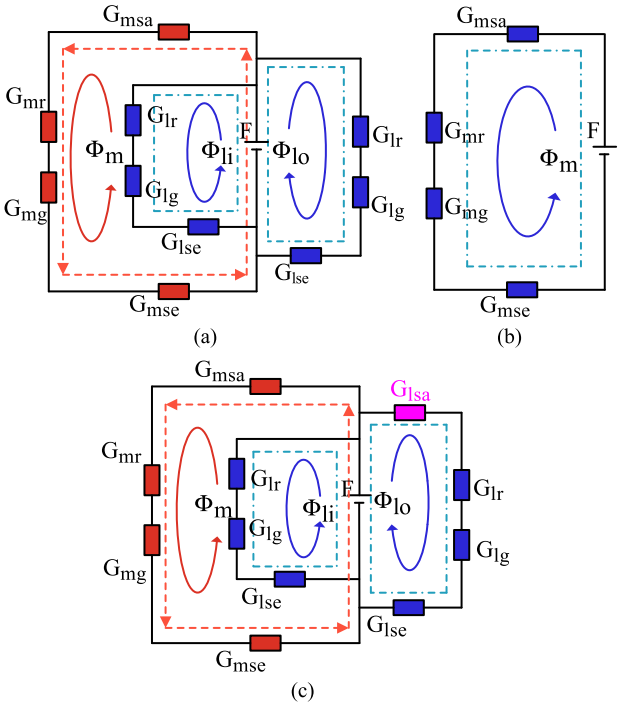

FIGURE 11. Equivalent magnetic circuit of three winding configurations, (a) WP-ES1; (b); EAA; (c) WP-ES2.

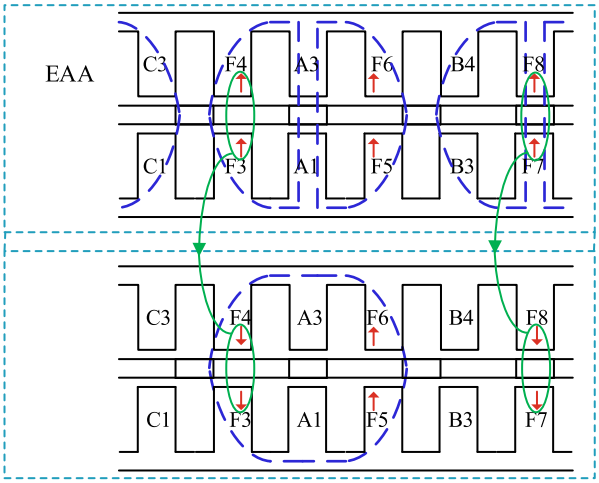

FIGURE 12. Reverse polarity of adjacent excitation windings of EAA.

the magnetic chain in that phase, and is therefore a beneficial leakage flux. In contrast, the two leakage flux loops of WP-ES1 are both non-beneficial leakage fluxes and do not contribute to the armature winding. Nevertheless, the EAA has a poor performance. Although the main flux path is shorter, it does not have a significant difference between the maximum and minimum flux value, mainly because there is not a large amount of flux passing through the armature winding when the rotor is aligned with the phase winding.

When the polarity of the adjacent excitation windings on the same side of the EAA type is opposite, the magnetic flux forms a closed loop between the excitation poles through the stator yoke, and the magnetic flux cannot be induced in the armature winding, which violates the intention of the magnetic flux flowing between the armature poles and the excitation poles, as is shown in Fig. 12.

Therefore, the directions of the magnetic potentials generated by the excitation windings on the two stators of the EAA must be the same, as shown in Fig. 10 (b). When the rotor is aligned with phase A, phase B and C will induce flux from their adjacent excitation windings, which results in a larger minimum value $\varphi_{\min}$ for the phase flux. And all the flux induced in the armature winding at this time is defined as leakage flux in WP-ES2. Instead of passing through the rotor aligned with the stator poles, the flux generated by the excitation winding passes over the edges of the rotor and forms a closed loop within its adjacent armature windings, resulting in a distribution of magnetic flux within the EAA armature winding that is evenly distributed, with no significant difference between the maximum and minimum flux.

The WP-ES2 does not completely circumvent the leakage flux as the EAA does, but achieves a reduction in leakage by reducing the number of polar opposite excitation stator poles. Unlike WP-ES1, when the rotor aligns with phase A, the leakage flux outside the main flux forms a closed loop in phase B, raising phase B $\varphi_{\min}$ a little, and also closes in phase A, raising phase A $\varphi_{\max}$. However, due to the magnetic voltage drop in the stator yoke, the contribution of the linkage

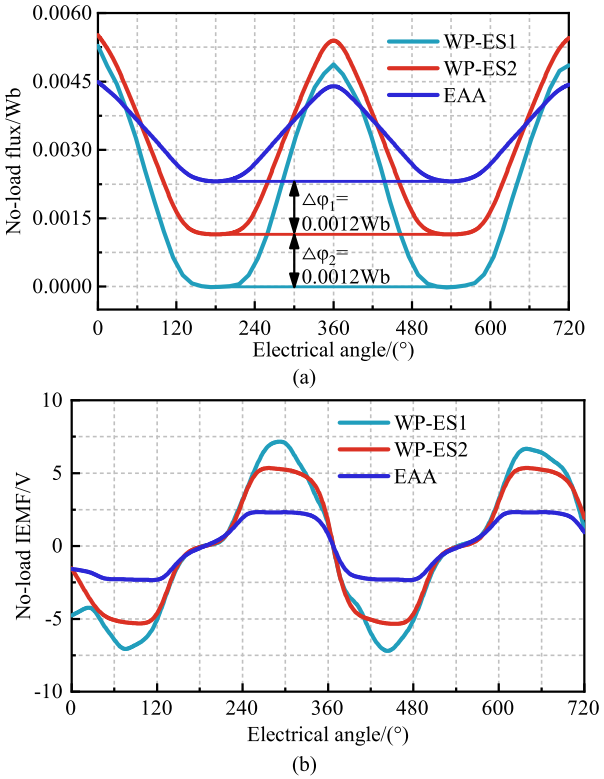

FIGURE 13. No-load curves for different winding configurations, (a) flux; (b) IEMF.

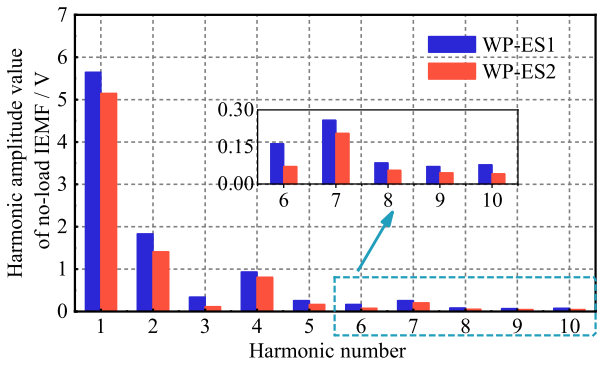

FIGURE 14. Comparison of winding partition harmonics.

to the maximum magnetic flux is smaller than that to the minimum magnetic flux, so the increase in φ_{max} is smaller than the increase in φ_{min}, which is reflected in the phase voltage of WP-ES2 being slightly smaller than that of WP-ES1 in terms of IEMF, and the curves of the three magnetic flux and back EMF are shown in Fig. 13.

The harmonic comparison between WP-ES1 and WP-ES2 is shown in Fig. 14. Since the proposed generator has a square ideal IEMF waveform, its total harmonic distortion is larger than that of the generator with sinusoidal waveform. As can be seen from the figure, the fundamental amplitude of WP-ES2 is 5.15 V, which is 0.5 V lower compared to 5.65 V of WP-ES1. However, in terms of harmonic characteristics, the

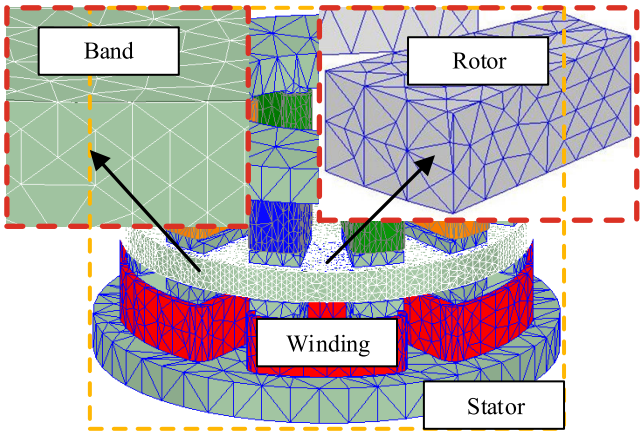

FIGURE 15. The 3D mesh of solved region.

first 10 harmonics of WP-ES2 are all reduced, with 5.02% lower total harmonics, 3.13% lower odd harmonics, and 4.5% lower even harmonics. As a result, the WP-ES2 has less harmonics in the no-load IEMF and higher quality of generation.

After the above analysis, when performing the winding arrangement, the alternating distribution of excitation and armature windings on the same side should be avoided in order to avoid the problem edge effect when the rotor is aligned with the stator slots, and also to avoid the problem of increasing the minimum value of the flux and reducing $\Delta\varphi$. The excitation and armature windings should be wound separately on the same side of the stator, so that when the flux linkage has a maximum value in one phase, the amplitude in the other two phases should be as small as possible, while reducing the effect of the edge effect.

IV. SIMULATION AND EXPERIMENTAL ANALYSIS

A. FINITE ELEMENT MAGNETIC FIELD SIMULATION

In order to verify the rationality of the topology, the electromagnetic characteristics of AFSDSG were studied. Thus, the three-dimensional topology model of the machine was established by ANSYS Electronics, and its flux linkage, phase voltage, and air-gap flux density were analyzed. The mesh is shown in Fig.15.

The flux linkage and IEMF curves of the three pole-slot configurations are shown in Fig. 16 for the winding arrangement WP-ES2. When the electrical angle is 240°, the rotor is aligned with the stator slot. Due to the edge effect, the flux linkage has begun to increase at this time, whereas the SPSS rotor is in line contact with the stator, and the PPSS and SPPS are in point contact, so φ_{SPSS} is the largest. As the rotor continues to rotate, the stator and rotor begin to overlap. In other words, during the period of 240° to 360° electrical angle, the overlapping area of the SPSS stator and rotor changes uniformly, and there is an obvious flat wave in the IEMF curve, at which point the phase is in a generating state. It can be seen from the above analysis that only when the overlapping area of the stator and the rotor changes linearly can the IEMF be a continuous constant value. Due to the less

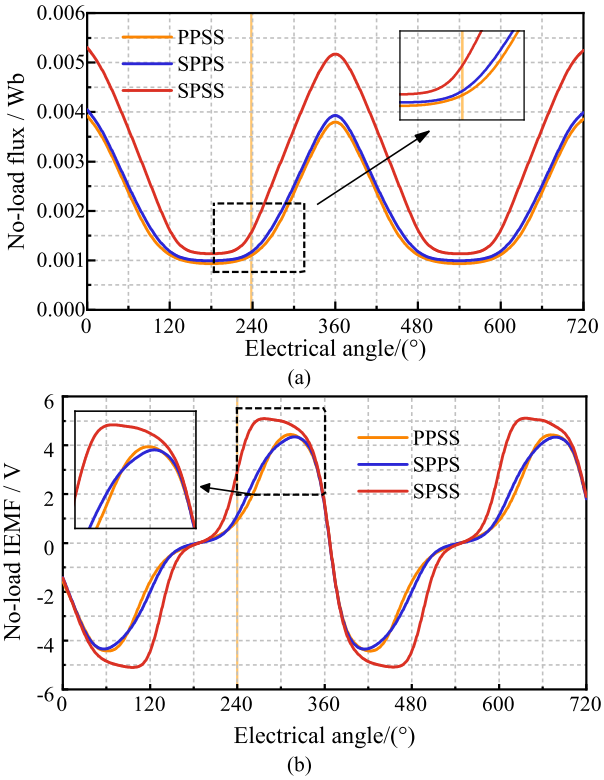

FIGURE 16. No-load waveforms, (a) flux; (b) IEMF.

linear variation in the overlapping area of the PPSS and SPPS, the voltage flat wave duration is shorter and the rectifier output voltage ripple is larger.

Fig. 17 shows the influence of the winding arrangement on the air gap magnetic flux density on the armature side based on SPSS. The leakage flux of WP-ES1 forms a closed loop in the excitation stator poles via the rotor, which has no effect on the armature winding, while WP-ES2 reduces the leakage flux in the excitation stator pole and increases the flux in the armature winding, which can increase the amplitude of the magnetic flux in the armature winding. The simulation waveforms verify the correctness of the previous analysis.

B. EXPERIMENTAL VERIFICATION AND COMPARATIVE ANALYSIS

To verify the validity of the above analysis, a prototype based on the SPSS pole-slot shape and WP-ES2 winding was fabricated according to the optimized parameters in Table 1, and experiments were conducted on the test bench. The prototype and the bench are shown in Fig. 18. The excitation current can be changed by adjusting the DC power supply and the generated power can output by a three-phase full-bridge rectifier. The rated speed of the generator was set at 3000 r/min for safety due to a laboratory experiment. Fig. 19 shows the phase IEMF waveforms of no-load and load for this prototype at 3000 r/min and 7500 r/min with the field current 5 A.

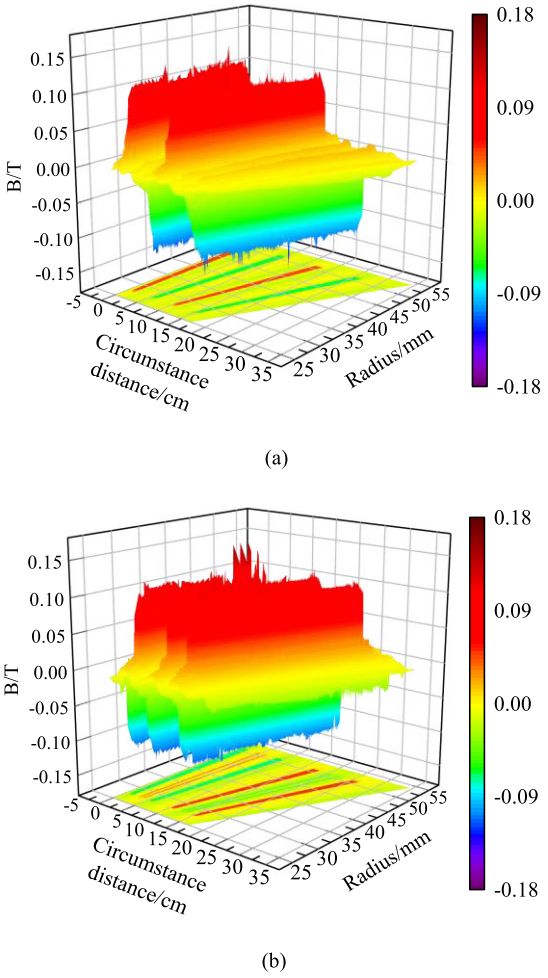

FIGURE 17. SPSS air gap magnetic density on the armature side for different winding configurations, (a) WP -ES1; (b) WP-ES2.

TABLE 2. Main parameters of the AFSDSG.

Parameter	Value
Outer diameter of stator yoke/mm	120
Inner diameter of stator yoke/mm	56
Outer diameter of stator pole/mm	104
Inner diameter of stator pole/mm	60
Outer diameter of rotor pole/mm	104
Inner diameter of rotor pole/mm	60
Axial length of rotor/mm	8
Axial length of single stator/mm	29.8
Turns of armature winding/turns	40
Turns of excitation winding/turns	40
Air gap length/mm	1
Number of segmental rotors	8
Number of stator poles	12
Core material	Pure iron DT4
Rotor material	Aluminium die casting

By maintaining the rated speed and adjusting the excitation current, the no-load characteristic diagram of the AFSDSG can be obtained as shown in Fig. 20 (a). As the excitation current gradually increases, the generator rectifier output

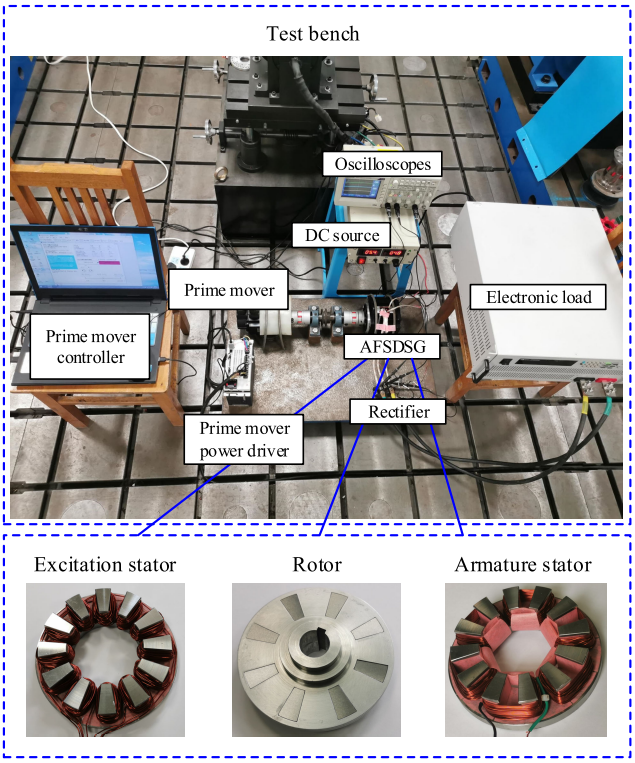

FIGURE 18. The prototype and test bench.

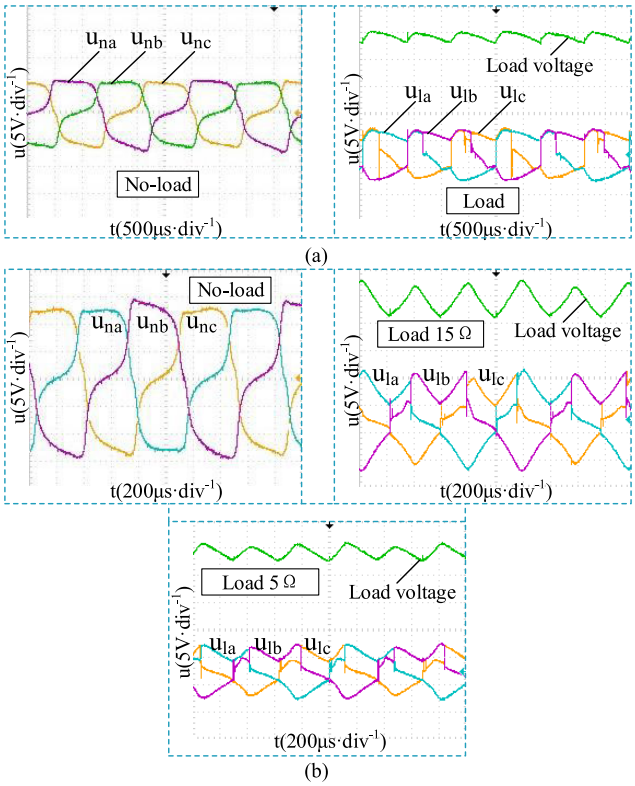

FIGURE 19. Experimental waveforms, (a) 3000rpm; (b) 7500rpm.

voltage gradually increases. As the excitation current gradually increases, the generator rectifier output voltage gradually increases. Fig. 20 (b) shows the external characteristics of the generator at rated speed and different excitation currents with

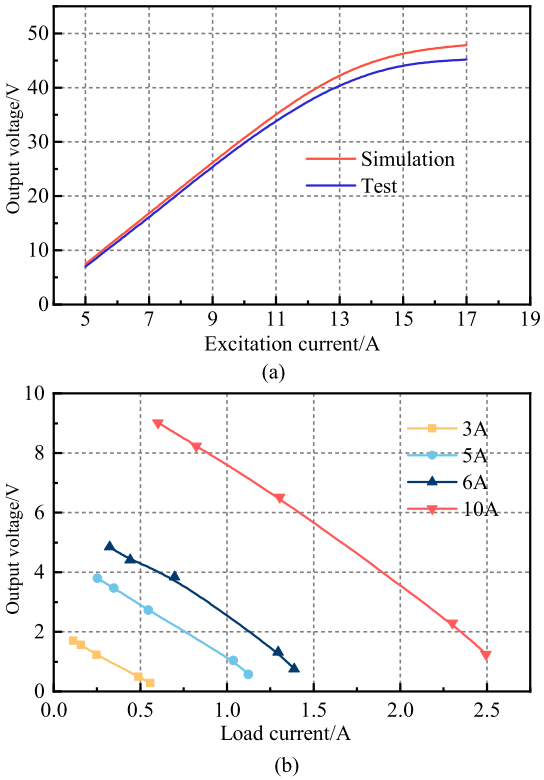

FIGURE 20. The characteristic curves, (a) No-load characteristic; (b) External characteristic.

different resistive loads, and the simulation results are in good agreement with the experimental results in terms of trend and amplitude, which verifies the reasonableness of the machine topology.

V. CONCLUSION

This paper presents a novel dual stators intermediate rotor flux axial flow AFSDSG for automotive applications to recover exhaust gas energy from turbocharger exhaust. The generator has a small mass rotor, which contributes to the high temperature resistance and low rotational inertia. The pole-slot shape of the stator, the rotor shape, the arrangement of the armature winding and the excitation winding are studied, and the finite element simulation analysis is compared with the experimental results to verify the above analysis, which provides the basis for the synergistic development of exhaust gas energy recovery and power generation technologies.

(1) The proposed generator is a double stator single rotor configuration with a rotating middle rotor that alternately induces flux in the armature windings. The machine has a sectorial pole-slot structure different from conventional sectorial poles parallel slots. It is because of the special pole and slot shape that the IEMF is positively related to the overlapping area of the stator and rotor, and when the variation of the area is constant with different rotor position, a constant IEMF is generated.

(2) It has been analyzed that the excitation winding and the armature winding should avoid alternate distribution on the

same side and that inter-pole leakage between the excitation should be minimized when the two are set on two stators respectively.

(3) Following on from the SPSS, it is analyzed that the WP-ES2 can reduce the excitation leakage compared to the WP-ES1 and increase the voltage amplitude by 49.03% compared to the EAA.

REFERENCES

[1] S. Hulagu and H. B. Celikoglu, "Environment-friendly school bus routing problem with heterogeneous fleet: A large-scale real case," *IEEE Trans. Intell. Transp. Syst.*, vol. 23, no. 4, pp. 3461–3471, Apr. 2022, doi: 10.1109/TITS.2020.3036696.

[2] V. M. Iyer, S. Gulur, G. Gohil, and S. Bhattacharya, "An approach towards extreme fast charging station power delivery for electric vehicles with partial power processing," *IEEE Trans. Ind. Electron.*, vol. 67, no. 10, pp. 8076–8087, Oct. 2020, doi: 10.1109/TIE.2019.2945264.

[3] J. Gao, L. W. Wang, and Y. C. Tian, "Numerical and experimental investigation of multi-halide chemisorption system for exhaust gas heat recycling," *Appl. Thermal Eng.*, vol. 194, Jul. 2021, Art. no. 117118, doi: 10.1016/j.applthermaleng.2021.117118.

[4] Z. Sun, Q. Xu, M. Cui, M. Nour, X. Li, D. L. S. Hung, and M. Xu, "Impact of flash boiling multiple injections timing on the combustion and thermal efficiency of a gasoline direct injection engine under lean-burn," *Fuel*, vol. 304, Nov. 2021, Art. no. 121450, doi: 10.1016/j.fuel.2021.121450.

[5] J. Cao, T. Li, and X. Zhou, "A study of smart thermal insulation coating on improving thermal efficiency in a marine two-stroke low-speed diesel engine," *Fuel*, vol. 304, Nov. 2021, Art. no. 120760, doi: 10.1016/j.fuel.2021.120760.

[6] C. Fei, Z. Qian, Z. Yang, J. Ren, S. Zhu, Y. Yan, and Z. Shu, "Combustion and emission performance of isopropanol-butanol-ethanol (IBE) mixed with diesel fuel on marine diesel engine with nano YSZ thermal barrier coating," *Energy*, vol. 256, Oct. 2022, Art. no. 124683, doi: 10.1016/j.energy.2022.124683.

[7] L. Sun, D. Wang, and Y. Xie, "Energy, exergy and exergoeconomic analysis of two supercritical CO_2 cycles for waste heat recovery of gas turbine," *Appl. Thermal Eng.*, vol. 196, Sep. 2021, Art. no. 117337, doi: 10.1016/j.applthermaleng.2021.117337.

[8] R. K. Golkhandan and H. Torkaman, "Reduction of induced shaft voltage and bearing current in turbo generators: Modeling, compensation, and practical test," *IEEE Trans. Ind. Electron.*, vol. 68, no. 5, pp. 4362–4372, May 2021, doi: 10.1109/TIE.2020.2985006.

[9] G. Xu, P. Hu, M. Song, Z. Wang, H. Zhao, and Y. Zhan, "Asynchronous operating ability of turbo generator with different field discharge resistors," *IEEE Trans. Ind. Appl.*, vol. 58, no. 2, pp. 1696–1705, Mar. 2022, doi: 10.1109/TIA.2022.3146111.

[10] D. Chen, Y. Zhang, and Y. Gu, "Online evaluation of turbo-generator shaft fatigue damage caused by subsynchronous oscillation," *IEEE Access*, vol. 8, pp. 55342–55353, 2020, doi: 10.1109/ACCESS.2020.2981509.

[11] S. A. Mirnikjoo, K. Abbaszadeh, and S. E. Abdollahi, "Multiobjective design optimization of a double-sided flux switching permanent magnet generator for counter-rotating wind turbine applications," *IEEE Trans. Ind. Electron.*, vol. 68, no. 8, pp. 6640–6649, Aug. 2021, doi: 10.1109/TIE.2020.3005106.

[12] H. Guo, X. He, J. Xu, W. Tian, G. Sun, L. Ju, and D. Li, "Design of an aviation dual-three-phase high-power high-speed permanent magnet assisted synchronous reluctance starter-generator with antishort-circuit ability," *IEEE Trans. Power Electron.*, vol. 37, no. 10, pp. 12619–12635, Oct. 2022, doi: 10.1109/TPEL.2022.3172339.

[13] R. R. Kumar, P. Devi, C. Chetri, A. S. S. Vardhan, R. M. Elavarasan, L. Mihet-Popa, and R. K. Saket, "Design and characteristics investigation of novel dual stator pseudo-pole five-phase permanent magnet synchronous generator for wind power application," *IEEE Access*, vol. 8, pp. 175788–175804, 2020, doi: 10.1109/ACCESS.2020.3025842.

[14] L. Kang and Y. Chen, "Optimal design of 9-phase permanent magnet synchronous generator with low voltage change rate for diesel railway vehicles," *IEEE Trans. Veh. Technol.*, vol. 71, no. 3, pp. 2681–2690, Mar. 2022, doi: 10.1109/TVT.2022.3140445.

[15] D.-H. Kim, K. S. Kim, I.-J. Yang, J. Lee, and W.-H. Kim, "Alternative bridge spoke permanent magnet synchronous generator design for wind power generation systems," *IEEE Access*, vol. 9, pp. 152819–152828, 2021, doi: 10.1109/ACCESS.2021.3127556.

[16] F. Yao, Q. An, and L. Sun, "Voltage stabilization analysis of a harmonic excitation generator employing armature current auxiliary self-excitation scheme under variable load conditions," *IEEE Trans. Ind. Electron.*, vol. 69, no. 6, pp. 5432–5441, Jun. 2022, doi: 10.1109/TIE.2021.3086730.

[17] S. Zhu, C. Liu, K. Wang, Z. Zhou, and J. Yu, "Structure and operating performance of a double electrical excitation synchronous generator with embedded brushless synchronous exciter utilizing DC-field excitation," *IEEE Trans. Energy Convers.*, vol. 37, no. 1, pp. 50–64, Mar. 2022, doi: 10.1109/TEC.2021.3096991.

[18] S. Zhu, Y. Hu, J. Li, C. Liu, and K. Wang, "Magnetic field analysis and operating characteristics of a brushless electrical excitation synchronous generator with DC excitation," *IEEE Trans. Magn.*, vol. 58, no. 8, pp. 1–7, Aug. 2022, doi: 10.1109/TMAG.2022.3148173.

[19] H. Geng, X. Zhang, L. Tong, Q. Ma, M. Xu, Y. Zhang, and L. Wang, "Performance optimization analysis of hybrid excitation generator with the electromagnetic rotor and embedded permanent magnet rotor for vehicle," *IEEE Access*, vol. 9, pp. 163640–163653, 2021, doi: 10.1109/ACCESS.2021.3133960.

[20] S. Pirzad, A. A. Ghadimi, A. H. Abolmasoumi, A. Jabbari, and S. Bagheri, "Optimal mixed control of axial flux permanent magnet synchronous generator wind turbines with modular stator structure," *ISA Trans.*, vol. 115, pp. 153–162, Sep. 2021, doi: 10.1016/j.isatra.2021.01.001.

[21] Z. Jun, L. Guanghua, C. Di, Z. Zhenyi, and L. Shuaihui, "Comparative analysis of coreless axial flux permanent magnet synchronous generator for wind power generation," *J. Electr. Eng. Technol.*, vol. 15, no. 2, pp. 727–735, Mar. 2020, doi: 10.1007/s42835-020-00359-z.

[22] S. Amin, S. Madanzadeh, S. Khan, S. S. H. Bukhari, F. Akhtar, and J.-S. Ro, "Effect of the magnet shape on the performance of coreless axial flux permanent magnet synchronous generator," *Electr. Eng.*, vol. 104, no. 2, pp. 959–968, Apr. 2022, doi: 10.1007/s00202-021-01338-x.

[23] M. A. N. Dehdez and J. Milimonfared, "A novel radial–axial flux switching permanent magnet generator," *IEEE Trans. Ind. Electron.*, vol. 69, no. 12, pp. 12096–12106, Dec. 2022, doi: 10.1109/TIE.2021.3128901.

[24] Y. Xu, M. Ai, Z. Xu, W. Liu, and Y. Wang, "Research on interior permanent magnet synchronous motor based on performance matching of electric bus," *IEEE Trans. Appl. Supercond.*, vol. 31, no. 8, pp. 1–4, Nov. 2021, doi: 10.1109/TASC.2021.3091062.

[25] W. Tong, L. Sun, S. Wu, M. Hou, and R. Tang, "Analytical model and experimental verification of permanent magnet eddy current loss in permanent magnet machines with nonconcentric magnetic poles," *IEEE Trans. Ind. Electron.*, vol. 69, no. 9, pp. 8815–8824, Sep. 2022, doi: 10.1109/TIE.2021.3111573.

[26] G. R. Bruzinga, A. J. S. Filho, and A. Pelizari, "Analysis and design of 3 kW axial flux permanent magnet synchronous motor for electric car," *IEEE Latin Amer. Trans.*, vol. 20, no. 5, pp. 855–863, May 2022, doi: 10.1109/TLA.2022.9693571.

[27] R. Wang, W. Liu, T. Meng, N. Jiao, X. Han, C. Sun, and Y. Yang, "Rotor position estimation method of brushless electrically excited synchronous starter/generator based on multistage structure," *IEEE Trans. Power Electron.*, vol. 37, no. 1, pp. 364–376, Jan. 2022, doi: 10.1109/TPEL.2021.3100361.

[28] M. A. J. Kondelaji and M. Mirsalim, "Segmented-rotor modular switched reluctance motor with high torque and low torque ripple," *IEEE Trans. Transport. Electrific.*, vol. 6, no. 1, pp. 62–72, Mar. 2020, doi: 10.1109/TTE.2020.2969356.

[29] S. Wang, K. Lin, M. Lin, Y. Kong, D. Xu, N. Li, and P. Wang, "Comparative study of E- and U-core modular dual-stator axial-field flux-switching permanent magnet motors with different stator/rotor-pole combinations based on flux modulation principle," *IEEE Access*, vol. 9, pp. 78635–78647, 2021, doi: 10.1109/ACCESS.2021.3078338.

[30] J. Liu, Q. Zhang, R. Wang, J. Hu, L. Zhang, and B. Cai, "An asymmetric-primary axis-flux hybrid-excitation generator for the vertical axis wind turbine," *IEEE Access*, vol. 9, pp. 92318–92325, 2021, doi: 10.1109/ACCESS.2021.3091466.

[31] W. Sun, Q. Li, L. Sun, and L. Li, "Development and investigation of novel axial-field dual-rotor segmented switched reluctance machine," *IEEE Trans. Transport. Electrific.*, vol. 7, no. 2, pp. 754–765, Jun. 2021, doi: 10.1109/TTE.2020.3033668.

[32] W. Ullah, F. Khan, S. Hussain, F. Alturise, M. Yousuf, and S. Akbar, "Consequences of flux gap on intriguing features of modular stator inset permanent magnet consequent pole synchronous machine," *IEEE Access*, vol. 10, pp. 49551–49565, 2022, doi: 10.1109/ACCESS.2022.3172305.

[33] J. Lai, J. Li, and T. Xiao, "Design of a compact axial flux permanent magnet machine for hybrid electric vehicle," *IEEE Trans. Ind. Electron.*, vol. 68, no. 8, pp. 6630–6639, Aug. 2021, doi: 10.1109/TIE.2020.3008358.

LINTAO LI received the B.S. degree from the College of Transportation, Ludong University, Yantai, China, in 2020. He is currently pursuing the M.S. degree with the School of Transportation and Vehicle Engineering, Shandong University of Technology, Zibo, China. His research interests include vehicle engineering, automotive electronics, design and manufacture of motor, and new energy electric vehicle technology.

LIWEI SHI received the M.S. degree in vehicle engineering from Shandong University of Technology, Zibo, China, in 2005, and the Ph.D. degree in electrical engineering and automation from Nanjing University of Aeronautics and Astronautics, Nanjing, China, in 2017. He primarily works on the research and development of vehicle's motor and electric vehicles with the School of Transportation and Vehicle Engineering, Shandong University of Technology. He has more than 50 authorized patents and released 30 papers and published two monographs. He obtained the second award of national technical invention and five items of the second prizes at provincial and ministerial levels.

ZHENGWEI LIU received the B.S. degree from the School of Mechanical and Electrical Engineering, Shandong Jianzhu University, Jinan, China, in 2021. He is currently pursuing the M.S. degree with the School of Transportation and Vehicle Engineering, Shandong University of Technology, Zibo, China. His research interests include vehicle engineering, automotive electronics, design and manufacture of motor, and new energy electric vehicle technology.

WENQIANG WANG received the B.S. degree from the School of Automobile and Traffic Engineering, Liaoning University of Technology, Jinzhou, China, in 2021. He is currently pursuing the M.S. degree with the School of Transportation and Vehicle Engineering, Shandong University of Technology, Zibo, China. His research interests include vehicle engineering, automotive electronics, design and manufacture of motor, and new energy electric vehicle technology.

FACHENG LI received the B.S. degree from the School of Transportation and Vehicle Engineering, Shandong University of Technology, Zibo, China, in 2021, where he is currently pursuing the M.S. degree. His research interests include vehicle engineering, automotive electronics, design and manufacture of motor, and new energy electric vehicle technology.